PROCEEDINGS REPRINT

SPIE–The International Society for Optical Engineering

Reprinted from

Space Astronomical Telescopes and Instruments II

13–14 April 1993
Orlando, Florida

Volume 1945

On-orbit sky background measurements with the FOS

R.W. Lyons, W.A. Baity, E.A. Beaver, R.D. Cohen, V.T. Junkkarinen, J.B. Linsky

Center for Astrophysics and Space Sciences,
University of California San Diego, 9500 Gilman Drive, La Jolla, Ca 92093-0111

R.C. Bohlin

Space Telescope Science Institute,
3700 San Martin Drive, Baltimore, Md 21218

ABSTRACT

Observations of the sky background obtained with the Faint Object Spectrograph during 1991-1992 are discussed. Sky light can be an important contributor to the observed count rate in several of the instrument configurations especially when large apertures are used. In general, the sky background is consistent with the pre-launch expectations and showed the expected effects of zodiacal light and diffuse galactic light. In addition to these sources, there is, particularly during the daytime, a highly variable airglow component which includes a number of emission lines. The sky background will have an impact on the reduction and possibly the interpretation of some spectra.

1. INTRODUCTION

When observing targets with the Faint Object Spectrograph (FOS) aboard the Hubble Space Telescope (HST), background counts from the sky are recorded in amounts depending on the instrument configuration. In the UV, the major sources of background light were expected to be emission lines from the ionosphere, notably Lyα (1216 Å), O I (1304 Å) and O I (1356 Å).[9] Diffuse galactic light may also be a contributing source. In the optical, the major sources of sky background at night were expected to be zodiacal light, diffuse galactic light, and individual faint stars, especially at low galactic latitudes.

Knowledge of the FOS sky background is necessary for several reasons. Normally, sky background measurements are not made during the course of an FOS observation. In most cases this background is not significant relative to the target flux. However, in cases where the largest aperture is used, knowledge of the background may be necessary to reduce the data properly. (The largest aperture has been used more than expected due to the poor point spread function of the HST.) This is also true for smaller apertures when the object is particularly faint. For faint targets, it may be necessary to know the contribution of the sky background before setting the target detection limits in order to insure proper target acquisition. The FOS is equipped with burst noise rejection software to remove cosmic ray noise. This software is activated by setting a parameter, REJLIM, equal to the maximum number of counts that may be recorded in an exposure frame before the frame is rejected. Because the sky background counts are included in this total, it is necessary to know their level when using REJLIM in order to avoid setting up the instrument in such a way that all the data are lost.

During Science Verification (SV) observations were made between February 1991 and March 1992 to investigate the character and positional dependence of the background sky light. These observations were made under three test proposal numbers:

SV2965 - high galactic latitude sky background test
SV2966 - low galactic latitude sky background test
SV2967 - low ecliptic latitude sky background test

Four instrument configurations were tested. The G160L grating was used with the Blue and Red Digicons. The prism and G650L grating were used with the Red Digicon. The results of these tests are presented in this report. No sky background tests had been carried out during the first test period after launch, Orbital Verification.

0-8194-1181-7/93/$6.00

2. OBSERVATIONS

2.1. Orbital geometry and observing constraints

The HST orbits the earth at an altitude of ~600 km (epoch 1991.5)[3] once every 96 minutes. The orbit is inclined to the equator by 28.5°. During any given orbit the telescope spends about 35 minutes in the Earth's shadow.

The relevant geometry is shown in the Figure 1 where the HST in its orbit is marked by a "◇".

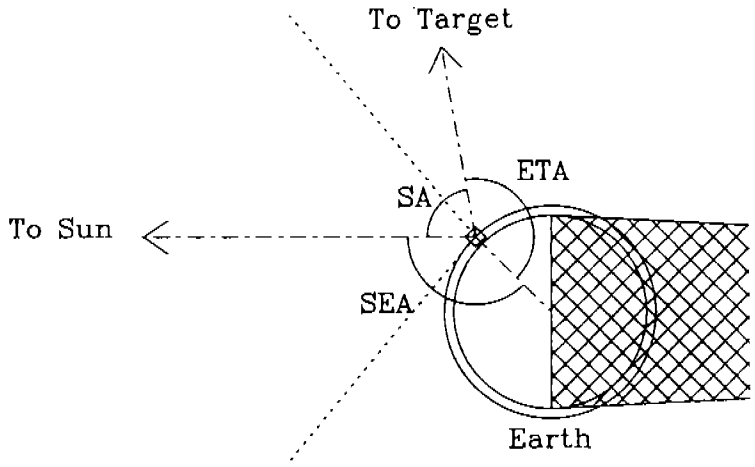

Figure 1: Orbital geometry (see text for definitions)

The Sun-Earth angle (SEA) is the angle subtended by the centers of the Sun and the Earth as seen from the satellite. When the Earth is directly between the HST and the Sun, this angle is 0°; when the HST is directly between the Sun and the Earth, the angle is 180°. Because of the orbital dynamics and the changing position of the Earth relative to the Sun, these values will not be reached on every orbit. For this paper we will assume that any results that depend on SEA are symmetric about the Sun-Earth axis and therefore SEA lies between 0° and 180°. Based on geometrical considerations, Sun-Earth angles less than about ~66° can be considered as nighttime. The twilight period is very short – less than one degree of Sun-Earth angle.

The Sun angle (SA) is the minimum angle between the Sun and the target as determined from the HST. No Sun angles much less than 60° were found in this data set. Except in special circumstances, the HST is restricted to targets more than 50° (dotted lines in Figure 1) from the unocculted Sun.[3]

The Earth-target angle (ETA) is the minimum angle between the center of the Earth and the target as seen from the HST. No targets were observed at angles much less than 90°. In other words, objects below the local HST horizon were not observed. In general, the minimum Earth-target angle for an object near the bright limb is 86° and 77° for one near the dark limb.[3]

2.2. Exposure details

The proposals did not indicate the specific areas of the sky that should be observed - instead they laid out criteria under which observations would be suitable. These criteria were designed so that the sky would be sampled at a number of positions at high and low galactic latitude and at low ecliptic latitude. Daytime observations were not ruled out. In some cases, when a verification test or science observation was completed and the conditions of scheduling permitted, the telescope was offset from the target just observed and sky readings were carried out using the FOS. In several instances, members of the Observation Support System (OSS) reported that the sky was not

free of source light or other faint targets. There was no requirement that tests with the Blue and the Red detectors be done on the same fields.

The exposures were made in the same manner for all the tests, but unlike other tests this differed for the two detectors. All exposures were made through the target acquisition aperture, also known as A-1, a 4".3 square. Target acquisition exposures (images of the aperture) were not made. Sky spectra were taken in the normal manner - that is, they were quarter-stepped (the spectra were shifted in one-quarter diode increments (pixels) along the array axis to improve the sampling) and overscanned (the spectra were shifted so that 5 separate diodes contributed to each pixel allowing the removal of effects due to disabled channels). In this manner, the 512 diode array produced readouts at 2064 positions. Known problem channels were disabled. The ACCUM mode was used so that the count array was only cleared after the last readout in an exposure, not after each intermediate one. Exposures were made only with the low dispersion configurations; the G160L grating was used with the Red and Blue Digicons, the G650L grating and the prism were used only with the Red Digicon. (See Section 3 for the configuration characteristics.) Each configuration produced 3 files. For the Blue side, the first file consisted of one 300 second exposure, the second, two exposures totalling 600 seconds, and the third, three exposures totalling 900 seconds. For the Red side, the first file consisted of two exposures totalling 300 seconds, the second, 5 exposures totalling 600 seconds, and the third, 7 exposures totalling 900 seconds. The total exposure time must be divided by 4 to get the exposure time per pixel. Most of the runs (one configuration, 3 files, on the Blue side or 3 configurations, 9 files, on the Red side) required more than one orbit to complete but all the observations in any given file were made without interruption. Runs and, in some cases, exposures crossed the day/night boundary. In all, 70 runs were made with the Blue detector and 68 with the Red.

The only other low dispersion configuration likely to be used for scientific observations is the prism and the Blue detector. This configuration was not tested. Some of the high dispersion configurations are affected by sky light but none of these were tested. No spectra were taken with the polarizer.

3. APPEARANCE OF THE SKY SPECTRA

A sample plot of the type of data obtained, by pixel and wavelength, is presented for each instrument configuration in Figure 2. The pixel range shown in the wavelength plot is indicated. Because the largest FOS aperture was used, the full width at half maximum for all features that are or look like emission lines is 48 pixels. (Many of the emission lines found in the sky spectra occur in regions where the sensitivity curve is a strong function of wavelength. Because these and subsequent spectra have been plotted with count rate as the ordinate rather than flux, these lines appear undistorted.) During Orbital Verification it was determined that the spectrum, as imaged on the diode array, would wander slightly because of an interaction with the Earth's magnetic field.[1] The pixel positions indicated below have been corrected for this effect, which is more pronounced in the Red detector than the Blue one.

When the Blue detector is used, the first order spectrum produced by the G160L grating covers the wavelength range from 1155 Å to 2508 Å at 1.7 Å pixel^{-1} (each diode responds to ~7 Å of spectrum). This spectrum covers pixels 1285 to 2063 (by convention here the first pixel is 0). It is bounded at the short wavelength end by two emission lines seen in the first order, geocoronal Lyα (the stronger) centered on pixel 1319 and O I λ1304 centered on pixel 1370. The spectrum is bounded at the long wavelength end by second order Lyα centered near pixel 2018. O I λ1356 was not seen on any of these spectra. This spectrum produced with this configuration in pixel and wavelength space is shown in the top row of Figure 2. The emission-like feature centered near pixel 627 is the zero order spectrum.

When the Red detector is used, the first order spectrum produced with the G160L grating covers the wavelength range from 1568 Å to 2424 Å. This spectrum covers pixels 0 to 497 where 0 is at the long wavelength end. The spectral coverage is reduced because the faceplate on the Red Digicon strongly absorbs light shortward of 1650 Å.[5] The output from this configuration (Figure 2 - row 2) typically shows one emission-like feature, the zero order sky spectrum centered near pixel 1418. In general we might expect the first order spectra taken with the two detectors to display similar characteristics since the wavelength coverage is similar. Where the coverage overlaps, the Red detector is more sensitive than the Blue one.

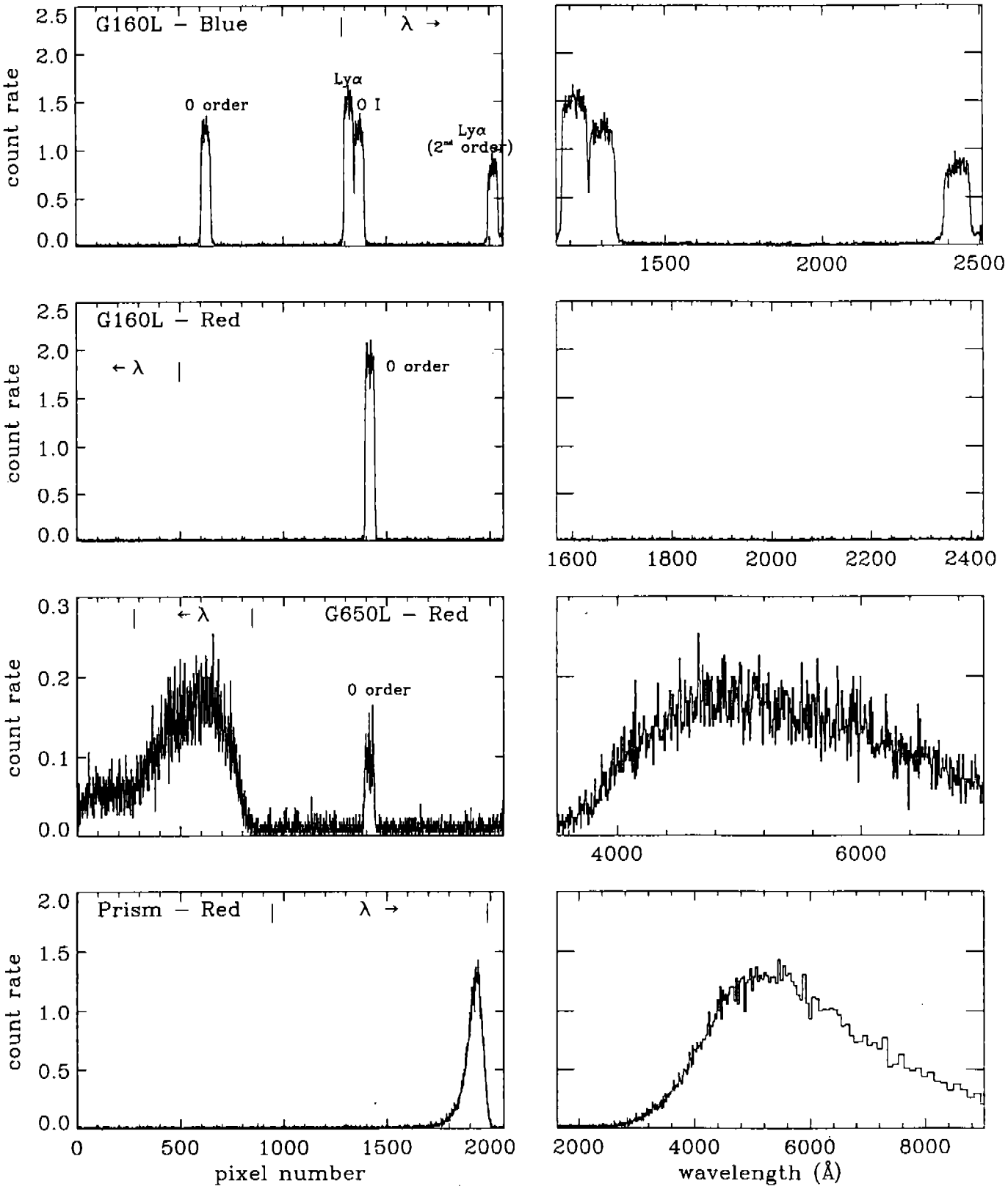

Figure 2: Typical sky spectra by detector readout position (pixel) and wavelength

The G650L grating used with the Red detector produces a first order spectrum which covers the wavelength range from 3500 Å to 7000 Å at 6.1 Å pixel^{-1}. Pixels 277 to 847 are used for this where 277 is at the long wavelength end. The HST-FOS efficiency curve indicates that the G650L grating has close to zero efficiency short of 3500 Å.[5] A typical sky spectrum produced with this configuration is shown in row 3 of Figure 2. The leading tail which is apparent short of pixel 277 is due to overlap from the second order spectrum. The emission line-like feature near pixel 1418 is the zero order spectrum.

A typical sky spectrum taken with the prism and the Red detector is shown in the bottom diagrams of Figure 2. This configuration produces a spectrum which runs from 1620 Å at pixel 944 to 9000 Å at pixel 1984. The dispersion varies from 0.4 Å pixel^{-1} at the short wavelength end to 116 Å pixel^{-1} at the long wavelength end. There is some overlap with the G160L spectra but the sensitivity is low. The region from 2400 Å to 3500 Å was not sampled with any other configuration. For the most part, the physical processes which produce the sky spectrum here should be similar to those which produce the G650L spectra. Note that, for each detector, the readout for the prism spectra is reversed relative to that for the grating spectra.

The only other low dispersion configuration likely to be used is the prism with the Blue detector. The sky spectra should be similar to those taken with the Red detector except that the count rate would be lower and the coverage would run from about 1500 Å to 6000 Å. The raw spectrum would be reversed relative to the Red detector.

4. DATA REDUCTION

The individual spectra were extracted from the accumulated spectra after correcting the latter for the effects of the diodes disabled during the run. For the G160L spectra taken with the Blue detector, mean count rates were determined for the peaks of the geocoronal Lyα and O I λ1304 lines. The mean count rate in the first order spectrum excluding these emission lines was also measured. The peak of the zero order spectrum and the mean count rate in the first order spectrum were measured for the G160L observations made with the Red detector. In order to quantify the G650L and prism spectra, a small number of pixels.(96 for the G650L and 24 for the prism) centered near the wavelengths of peak count rate (4912 Å for G650L and 5068 Å for the prism) were averaged together. The mean values for the observed spectra were also found. For each exposure, the mean background for a region with no external sources (i.e. the dark background) was determined by averaging the pixel counts in the regions clear of obvious features. No corrections were made for the image motion mentioned in the previous section. However, the pixel ranges of the emission-like features were restricted to remove the impact of any motion that would affect the line edges.

The positions (right ascension and declination) of the Sun during the exposure and the target were obtained from the science header file provided as was the angular distance between the Sun and the target as seen from the HST (SA). These are essentially constant during an observation run. The right ascension and declination of the Earth relative to the HST during each observation were computed from the orbital parameters contained in the science header file using a program (HSTPOS) written by Tom Ake of the GHRS group, modified by Fred Walter and adapted locally for the FOS science header format. This position was then used to compute the angular separation between the Sun and the Earth (SEA) and the Earth and the target (ETA) for each observation. The ecliptic coordinates of the Sun and target, and the galactic coordinates of the target were computed.

5. DARK BACKGROUND

The "dark background" is the background that would be recorded whether or not the FOS was actually exposing on any target. Previous work[8] has shown that this background arises from Cerenkov radiation emitted from high energy particles crossing the Digicon faceplate. Under certain conditions the whole diode array can record counts. In general, the dark background count rate is a function of the geomagnetic latitude. At low geomagnetic latitudes, the average dark background is ~0.01 counts sec^{-1} pixel^{-1} for the Red detector and ~0.008 counts sec^{-1} pixel^{-1} for the Blue one. On average, the count rate is about 3 times larger when the HST is near the geomagnetic extremes of its orbit. (We are ignoring the South Atlantic Anomaly where the larger average number of energetic particles creates so many counts that observations are suspended.) When a large number of background observations are summed, there is some large scale structure apparent across the array. The peak-to-peak variations are around 15% for the

Blue detector and 5% for the Red.[7]

As indicated earlier, the dark background was measured in regions free of exposure from external sources. The few cases where there was a notable discrepancy between these measures and the results expected involved the appearance of intermittent noisy channels. Because they were intermittent, they were not normally disabled.

6. SKY BACKGROUND

We find no obvious peculiarities in any of the four runs in which the OSS reports indicated possible contamination by visible sources. Since target acquisition exposures were not made, we cannot examine these to determine whether or not discrete objects were present in the sky field. However, since discrete objects do not fill the aperture uniformly as the sky does, it is possible to use the zero order spectrum, when it is available, to check for the presence of any objects that might affect the sky field. Ten fields were identified which had discrete sources. These fields were removed from the data under consideration. Several other fields may be contaminated slightly.

6.1. G160L with the Blue Digicon

Over the course of the test, observations were made at almost the full range of Sun-Earth angles. Excluding the prominent emission lines noted in Section 3, only one run shows an obvious first order spectrum. It is present at about the same levels in all three files (0.015 counts sec^{-1} $pixel^{-1}$ above the background). Some other runs hint at a sky presence but the low number of counts (less than ~5 counts $pixel^{-1}$ for almost all files) makes it hard to tell whether these are real or just random effects from the Cerenkov noise. Based on the shape of the mean dark background discussed earlier, we would expect about 5% fewer dark counts in the region measured for the dark background than in the region measured with the first order sky spectrum. After adjusting the measured backgrounds by this amount we find a mean residual count rate in the first order spectrum of $1.42 \times 10^{-3} \pm 2.39 \times 10^{-3}$ counts sec^{-1} $pixel^{-1}$.

The emission line intensities depend mainly on the angular distance between the Sun and the Earth as seen from the HST (SEA) since this determines the illumination of the local atmosphere. Figure 3 shows the variation in the count rates of Lyα and O I λ1304 as a function of the Sun-Earth angle (SEA). The values have been corrected for the mean dark background near the lines. Lyα is always present, producing a minimum count rate of about 0.2 counts sec^{-1} $pixel^{-1}$ at 0° and a maximum about 2 counts sec^{-1} $pixel^{-1}$ at 180°. O I is somewhat more sensitive to the Sun's relative position, being essentially zero for angles less than 80°. One run produced what appears to be an unusually high count rate for O I, about 0.6 counts sec^{-1} $pixel^{-1}$ higher than average. These data, taken on 23 March 1991, were probably affected by the major solar activity at that period.[2] The second order Lyα line is approximately half the strength of the first order feature.

There is a considerable spread in the count rates at any given Sun-Earth angle. For any given run (6 exposures), the Sun-target angles (total range for all runs 50-180°) do not change by much. The Sun-Earth angles and the Earth-target angles (total range from all runs 70-180°) often undergo considerable change especially when the run is spread over more than one orbit. (The ranges represented by the data in any given file depend on the total exposure time for the file and the position of the telescope in its orbit.) At small Sun-Earth angles, the count rate varies inversely with the Sun-target angle – larger angles result from pointing directions more towards or into the Earth's shadow. When the atmosphere is well illuminated (SEA large), the Earth-target angle is more important, with smaller angles producing a higher count rate.

These results are consistent with those obtained from GHRS data for geocoronal Lyα.[10,11]

The highest count rate found for the zero order spectrum was ~1.6 counts sec^{-1} $pixel^{-1}$, obtained during the daytime. The nighttime rates ranged between 0.2 and 0.6 counts sec^{-1} $pixel^{-1}$.

6.2. G160L with the Red Digicon

The spectral coverage of the Red detector with the G160L overlaps that of the Blue detector but doesn't extend

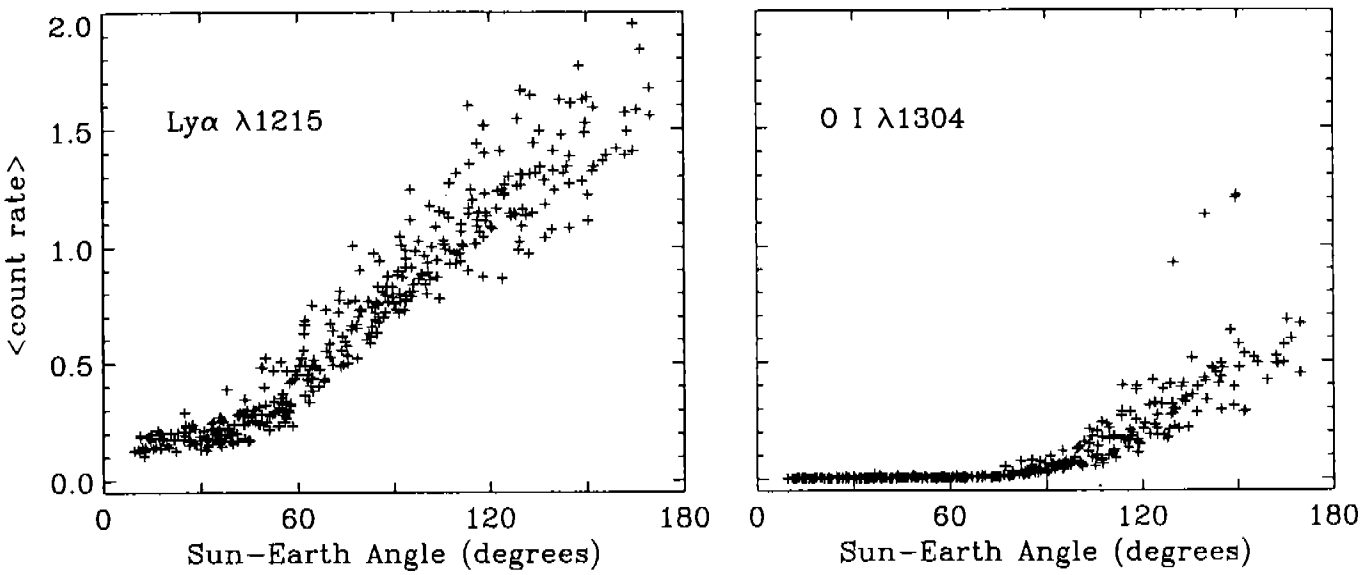

Figure 3: Count rates for Lyα and O I λ1304

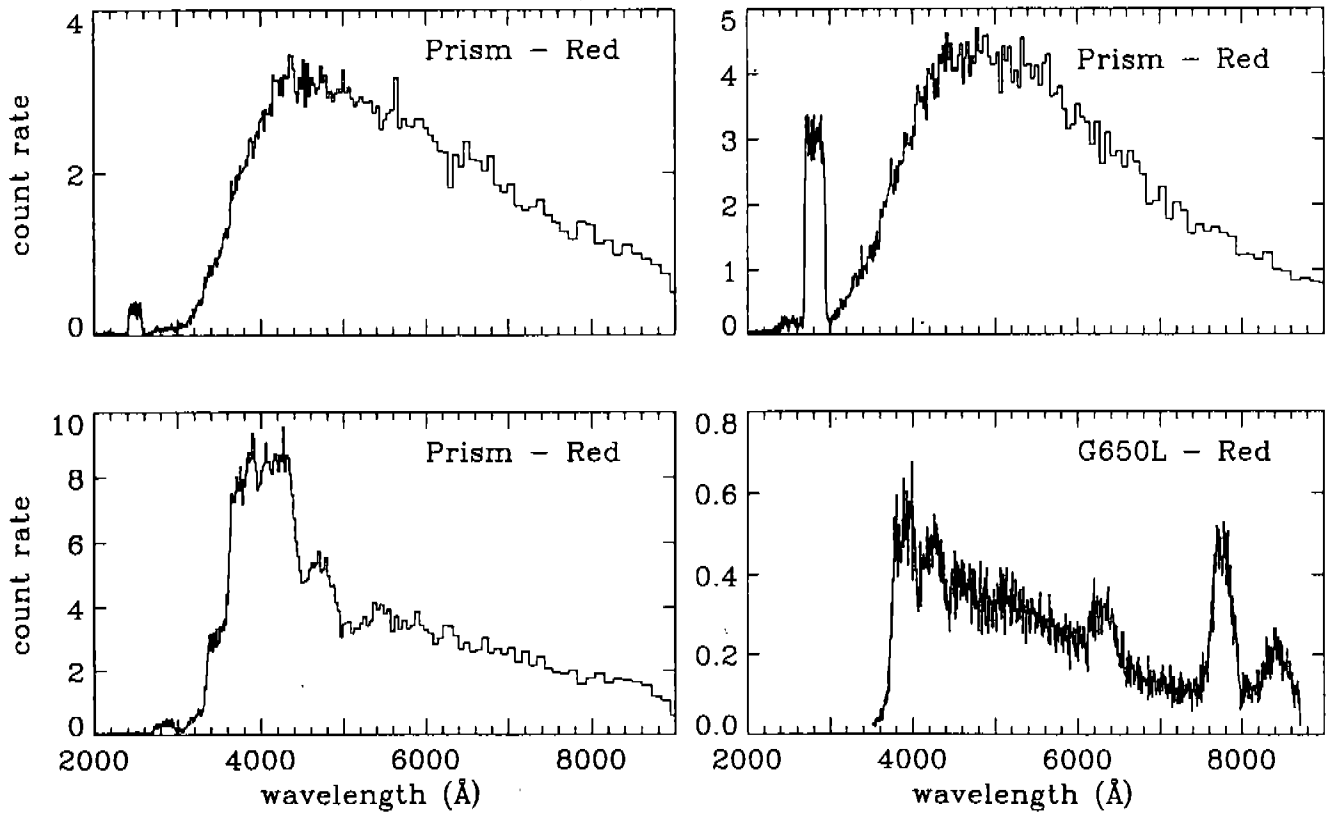

Figure 4: Some anomalous daytime sky spectra

as far to the blue. Unlike the previous case, there were a number of observations in which a first order spectrum is clearly present, appearing as a noisy continuum rising from the dark background near 2 counts pixel^{-1} at the short wavelength edge of the spectrum to around 6-7 counts pixel^{-1} at the long wavelength end during a 900 second exposure (225 seconds for each pixel). For these cases, the mean rate exceeded the background by 0.01 counts sec^{-1} pixel^{-1}. Perhaps the larger number of detections was just fortuitous but the Red detector, while it does have a higher dark background rate, is also more sensitive than the Blue detector. In addition there were a number of observations in which the results were very suggestive but the higher noise level makes it harder to separate these from the random effects of the Cerenkov noise. The total number of counts per pixel was similar to that found with the Blue detector because the exposure time between readouts was shorter. In this case, the expected difference between the dark count rates in the background and spectral regions was less than 1%. We find a mean residual count rate in the first order spectrum of $1.74 \times 10^{-3} \pm 3.16 \times 10^{-3}$ counts sec^{-1} pixel^{-1} above the background.

The highest count rate found for the zero order spectrum was ~8.7 counts sec^{-1} pixel^{-1}. This rate was obtained during the daytime. The nighttime rates ranged between 1 and 3.5 counts sec^{-1} pixel^{-1}.

6.3. G650L and prism spectra

While the wavelength range covered by the prism extends somewhat farther to the blue than that covered by the G650L, the spectra produced by these two configurations are relatively similar and will therefore be treated together. They should be produced by similar processes. The weakness of the UV spectrum implies that the zero order spectrum present in the G160L exposures taken with the Red detector also result from those processes. On the other hand, the zero order spectrum obtained when the Blue detector is used will also be affected by the geocoronal Lyα and O I emission lines.

In general, the count rates at the peak behaved similarly in the day and night sky. The count rate did show a slight increase in the daytime sky. However, in some cases the peak count rates were substantially higher and/or showed considerable variations over the time scale of the run. An examination of the Sun-Earth angles showed that the results for a particular patch of sky showed the greatest inconsistencies when daytime observations were included. Visual inspection of the sky spectra revealed the presence of highly variable emission features in some daytime sky spectra.

From the data available for the G650L Red detector spectra, the count rate from the entire array ranged between 15 and 107 counts sec^{-1}. Coincidentally, the mean count rate pixel^{-1} in the zero order spectrum turned out to be very similar to the average count rate pixel^{-1} for the first and second orders combined.

The FOS efficiency curves[5] indicate that the prism configuration is ~3 times more efficient than the G650L configuration. While the count rate difference at the peak is greater than this factor would indicate, the spectra are compatible with what one would expect when allowance is made for the rapidly decreasing dispersion of the prism at longer wavelengths. For this data set, the count rate obtained from the entire array ranged between 20 and 267 counts second^{-1}.

6.3.1. Daytime G650L and prism spectra

Some of the more extreme cases of anomalous daytime sky spectra are shown in Figure 4. Continuum changes are evident in a number of the other spectra and some obviously have unresolved structure. We estimate that the unassigned wavelengths given below have uncertainties of at least ±12 Å.

Some of the daytime prism spectra showed O II λ2470 (Figure 4 top left).[5] A few showed a highly variable emission line, ~2812 Å (Figure 4 top right). These two lines did not tend to occur together. The prism spectra showed several other lines as well. One of these, Figure 4 bottom left, shows what is probably a single emission (it only covers 48 pixels) centered near 3950 Å. Most of the lines present in the G650L spectrum (Figure 4 - bottom right) are not noticeable in the prism spectra because they occur at long wavelengths where the resolution is very poor.

Compare the G650L spectrum in Figure 4 with the one presented in Figure 2. Note that the wavelength range is larger in Figure 4 because the region of second order overlap has been included. A number of emission lines are evident. Two lines, λ3900 (perhaps N_2^+ λ3914) and λ4230 distort the spectrum at the short wavelength end. Few of our sky spectra show these particular lines. O I λ7774 is present together with O I λ6300. In our spectra it appears that O I λ6300 only occurs when O I λ7774 is present. In the spectrum shown, O I λ7774 is enhanced because of the overlap from the second order of λ3900. The feature shown near λ8430 (O I λ8446?) only appears when λ3900 and λ4230 are present. λ6573, probably Hα, occurs in several spectra apparently unaccompanied by other emission lines. On a few spectra when both O I λ7774 and O I λ6300 are present λ7320 also appears.

6.3.2. Zodiacal light

The contribution due to the zodiacal light depends on the angular separation between the target and the sun along the ecliptic (heliocentric ecliptic longitude $\lambda - \lambda_\odot$) and the distance of the target from the ecliptic (ecliptic latitude β). It is present at some level across the whole sky.[6]

In Figure 5, we have plotted the prism's average count rate at the peak corrected for the dark background against heliocentric ecliptic longitude (folded onto a 180° scale) for two ranges of ecliptic latitude. The +'s denote points at ecliptic latitudes outside ±50° while the x's denote ecliptic latitudes within 10° of the ecliptic. Results for the intermediate latitudes lie between the results for the two ranges plotted. The plot on the left shows the results for all the relevant data (both day and night) taken with the prism. Each run has 14 exposures and the variation in the peak count rate for some runs is clear. The plot on the right shows the same results but the daytime data have been excluded. It is apparent that including the daytime data adds greatly to the scatter.

The nature of the count rate variations are typical of those expected from the zodiacal light. The count rate increases as targets closer to the ecliptic are used and the heliocentric ecliptic longitude decreases. A small rise in the count rate occurs in the anti-solar region. Since HST observations are generally not carried out within 50° of the Sun, there are no low ecliptic latitude points (x's) at small heliocentric ecliptic longitudes. However, since it is possible to observe more than 50° above or below the Sun, measurements can be made in this region (+'s). No additional information can be derived by examining the G650L spectra or the G160L red spectra since the same targets were used for all three sets of observations. Because the G650L configuration is not as sensitive as the prism configuration, the count rate at 60° heliocentric ecliptic longitude within 10° of the ecliptic is lower, ~0.6 counts sec^{-1} $pixel^{-1}$.

6.3.3. Diffuse galactic background

Diffuse galactic light depends on the position of the target relative to the galactic center and can be characterized through the use of galactic coordinates. The galactic center is at the origin and longitude is specified running along the galactic plane. This component should be smaller for targets farther away from the galactic plane. In general, outside of the galactic plane, the contribution of the diffuse galactic light to the sky background should be less than that of the zodiacal light.

Figure 6 shows the average count rate at the peak for the G650L and the prism spectra ignoring the daytime observations and observations where the zodiacal light is important. Each symbol represents the average value of the relevant points for each run. While the galactic longitude is a factor, we will ignore it here because of the small number of observations. As expected, the count rate is higher at small galactic latitudes.

6.4. Pre-launch sky background predictions

The expected relationship between sky background sources and the Digicon count rate (N_λ) is presented in Table 4.3-1 of the FOS Instrument Handbook.[4] In these formula, E_λ is the combined HST+FOS efficiency for the grating configuration of interest. *Ap* refers to the aperture area in square arc seconds. Unlike most of the other apertures available with the FOS, the 4.″3 square aperture used during these tests is considerably larger in size than an individual diode. The effective aperture for these tests thus becomes 4.″3 by 1.″4 since the diodes are only 1.″4 high.

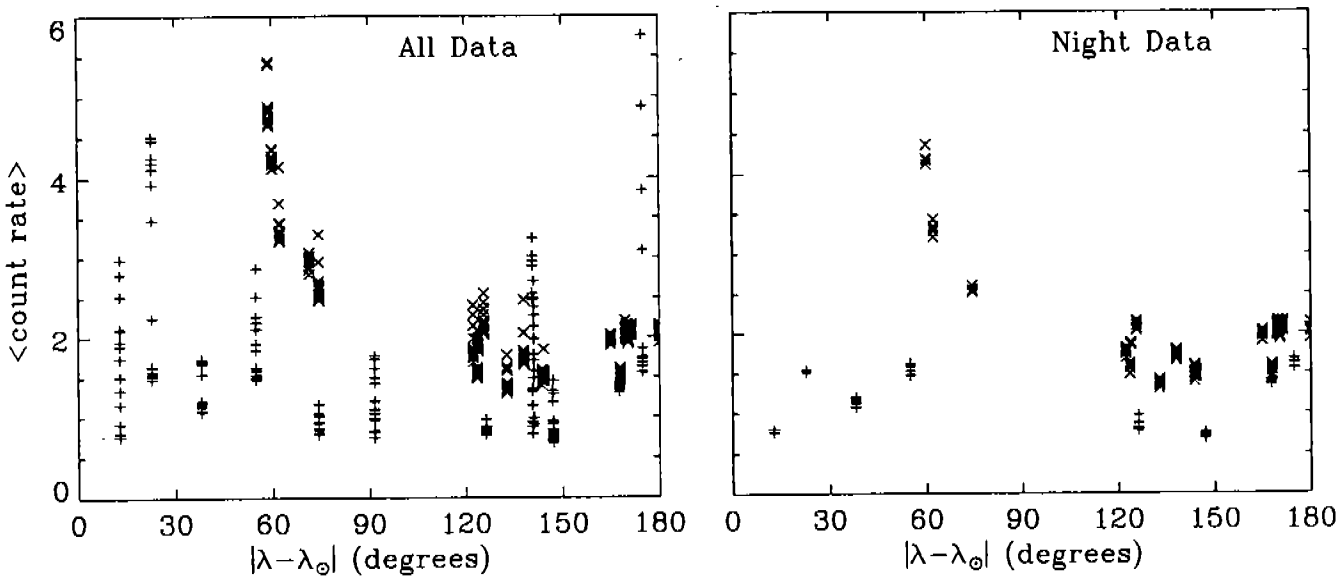

Figure 5: Zodiacal light – prism count rate in peak region (x : $|\beta| \leq 10°$, + : $|\beta| \geq 50°$)

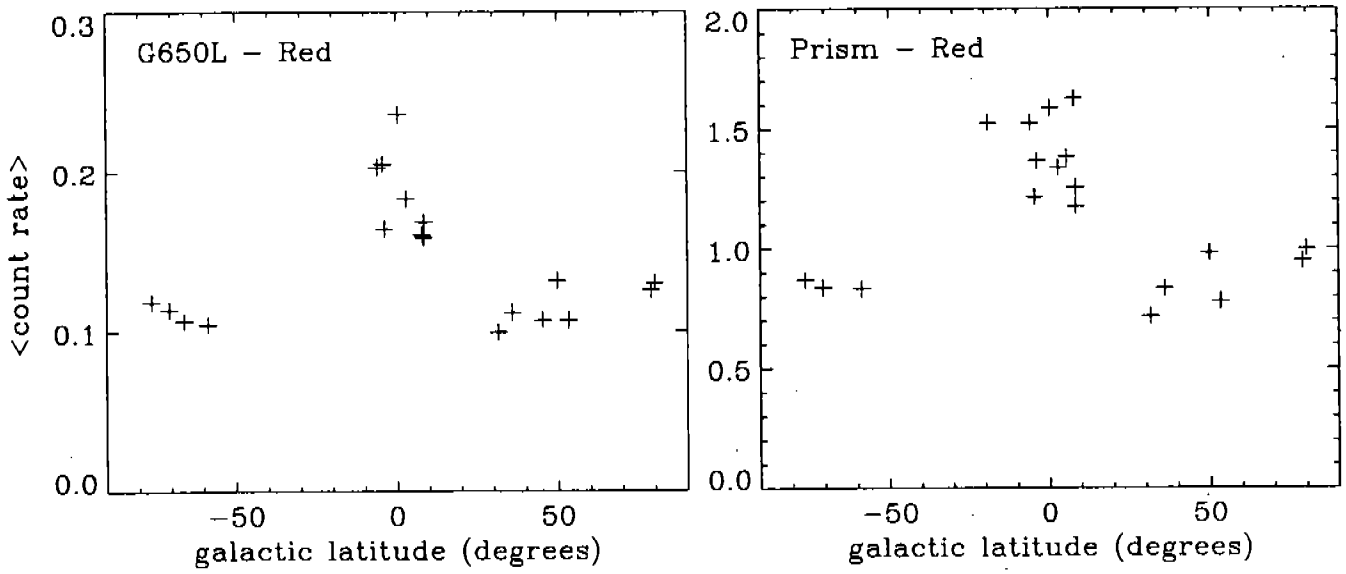

Figure 6: Diffuse galactic light – count rate in peak region for G650L and prism

Table 4.3-1 includes a formula for calculating the count rate for the airglow lines. The efficiency of the configuration at Lyα is $\sim$1.1 x 10^{-3}. The count rates predicted, 1.75 at noon and 0.2 at midnight, are similar to those found observationally. At Lyα, 1 count sec^{-1} $pixel^{-1}$ is equivalent to a flux of $\sim$7.3 x 10^{-14} erg cm^{-2} sec^{-1} $Å^{-1}$. For O I, the efficiency is $\sim$2.5 x 10^{-3}. The predicted count rate at noon, 0.38 count sec^{-1} $pixel^{-1}$, is lower than these data indicate. There is however quite a spread, some of which may depend on solar activity. At O I, 1 count sec^{-1} $pixel^{-1}$ is equivalent to a flux of $\sim$3.1 x 10^{-14} erg cm^{-2} sec^{-1} $Å^{-1}$.

The zodiacal light is a function of the heliocentric ecliptic longitude and the ecliptic latitude. The formula shown approximates the solar spectrum source function with a Planck distribution of 5770° K. The diffuse galactic light is a function of b, the galactic latitude. It is also a function of the galactic longitude but this dependence has not been included in the formula provided. Models of the sky spectrum expected from the zodiacal light and the diffuse galactic background were computed for both instrument configurations. The observed count rates at night were comparable to the count rates expected based on these formulae.

7. CONCLUSIONS AND RECOMMENDATIONS

The continuum and the emission lines from the sky background can contaminate the spectra of faint objects. For example, with the 1″ aperture, after the installation of COSTAR, the G650L spectrum shown in Figure 4 will peak at roughly 0.055 counts sec^{-1} $pixel^{-1}$. This will contribute about 35% of the counts near 4000 Å in the spectrum of a 20^{th} magnitude quasar. Any emission lines from the sky might be hard to separate from those produced by the object. The problems are much worse with the larger apertures. In addition, there is considerable short term variation in the strength and character of the sky spectrum, particularly during the HST daytime. When the exposure is broken up into a number of pieces, changes between the pieces may be sufficient to identify sky features.

For the G160L operating with the Blue detector, the strengths of the geocoronal Lyα and O I λ1304 correlate well with the the Sun-Earth angle. The strength of Lyα agreed well with the predictions. It is always present at some level but can be minimized by observing at small Sun-Earth angles. The O I line which proved to be slightly stronger, in several cases much stronger, than expected, can be reduced to levels near zero by observing at Sun-Earth angles $\leq 80°$. Observers who wish to use spectra taken in this region should use a small aperture to reduce contamination by this feature in the event the observation cannot be scheduled as desired. If the target acquisition aperture is used, a check of the raw spectrum may help interpret the results. Since the inverse sensitivity curve varies quite strongly in this region, these lines become highly distorted in flux-calibrated spectra.

Weak but definite spectra have been recorded in the first order with the G160L operating with both the Blue and the Red detectors. Any further investigation of this should probably be carried out with the Red detector since the higher sensitivity has yielded a larger number of definite detections.

The count rates from the zodiacal light and diffuse galactic background are similar to what was expected for the night sky.

The prism was not tested in combination with the Blue detector. A comparison between the inverse sensitivity curves of the prism with the two detectors indicates that observations made with this configuration will probably need to be corrected for the sky, especially if the target acquisition aperture is used.

Allowances will need to be made by anyone using the burst noise rejection software. If the aperture or frame time is not small enough or the relevant diodes are not disabled, great care will need to be taken to avoid setting the rejection parameter, REJLIM, too low, thereby losing all the data. We recommend exploration of an observing strategy in which diodes affected by well defined features can be temporarily added to the disabled diode table by observers who wish to take advantage of the burst noise rejection option. With the current observing procedures an observer can at best specify a limited range of diodes that can be active. Activating REJLIM will cost the observer any background information or spectrum that might be available outside of that range. Observers who wish to use REJLIM during daytime observations that include the visible portions of the spectrum should be discouraged due to the variable nature of the airglow features.

These tests were run with the largest FOS aperture. After COSTAR is installed, science observations will probably use the small apertures exclusively. The small aperture results can be obtained by scaling, but some tests to verify the scale factors may be in order. The polarizer will no longer be available.

Observations made with the FOS and the GHRS may be of use to scientists interested in the characteristics of the Earth's upper atmosphere.

8. ACKNOWLEDGEMENTS

The authors would like to thank Fred Walter for supplying copies of his GHRS work on the geocoronal Lyα line and copies of his software and Walker Fillius for telling us of the solar activity in late March, 1991.

This research was supported by NASA NAS5-29293 and NAG5-1630 which are greatly appreciated.

9. REFERENCES

1. Baity, W.A., Beaver, E.A., Cohen, R.D., Junkkarinen, V.T., Lyons, R.W., Fitch, J., Hartig, G.F., Lindler, D.J. 1993 "Performance of the FOS Detectors in a Variable External Magnetic Field ", these proceedings.

2. Blake, J.B., Kolasinski, W.A., Fillius, R.W. Mullen, E.G. 1992 "Injection of Electrons and Protons with Energies of Tens of MeV into L<3 on 24 March 1991", Geophys. Res. Lett. **19**, 821.

3. Bond, H (ed.) 1992 "Hubble Space Telescope Cycle 3 Call for Proposals", published by Space Telescope Science Institute, May.

4. Ford, H., Hartig, G. 1990 "Faint Object Spectrograph Instrument Handbook - Version 1.1", published by Space Telescope Science Institute, May.

5. Kinney, A. 1993 "Hubble Space Telescope Faint Object Spectrograph Instrument Handbook - Version 4", published by Space Telescope Science Institute, February.

6. Levasseur-Regourd, A.C., Dumont, R. 1980, *Astron. Astrophys.*, **84**, 277.

7. Lyons, R. W., Baity, W. A., Beaver, E. A., Cohen, R. D., Junkkarinen, V. T., Linsky, J. B., and Rosenblatt, E.I. 1992 "Faint Object Spectrograph On-Orbit Dark Background Measurements", FOS Instrument Science Report CAL/FOS-080, August.

8. Rosenblatt, E.I., Beaver, E.A., Cohen, R.D., Linsky, J.B., Lyons, R.W. 1991 "Cerenkov Background Radiation in Imaging Detectors", in Proceedings of SPIE - *Electron Image Tubes and Intensifiers II*, Csorba, I.P. (ed.), (Bellingham, WA) **1449**, 72.

9. Paresce, F., Volpe, R., Albrecht, R. 1984 "The Background Radiation Model for the Space Telescope"

10. Walter, F. M. 1990 "The GHRS Spectrum of Geocoronal Lyman α", GHRS Cal/SV Report, 30 Oct.

11. Walter, F. M. 1991 "Further Measurements of the Geocoronal Background", GHRS Cal/SV Report, 30 Jan.